University of Oxford

Score-Based Diffusion Models for Protein Backbone Generation

by

Yuanhao Jiang

Wolfson College

A dissertation submitted in partial fulfilment of the degree of Master of Science in Statistical Science.

Department of Statistics, 24–29 St Giles,
Oxford, OX1 3LB

September 2025

This is my own work (except where otherwise indicated)

Candidate: Yuanhao Jiang

Signed:.....

Date:.....

Abstract

The abstract should go here.

Acknowledgements

I would like to thank the following:

Contents

1 Introduction **1**
- 1.1 Background on Diffusion Models . . . 1
- 1.2 Motivation: Protein Structure Generation . . . 1
- 1.3 Diffusion Models for Protein Structures . . . 1
- 1.4 Structure of the Dissertation . . . 2

2 Score-Based Diffusion for Generative Modelling **3**
- 2.1 Background and Motivation . . . 3
- 2.2 Forward Diffusion Processes . . . 3
  - 2.2.1 Discrete-Time Formulation . . . 4
  - 2.2.2 Continuous-Time Formulation . . . 4
- 2.3 Reverse-Time Diffusion Processes . . . 6
  - 2.3.1 Discrete-Time Reverse Process . . . 6
  - 2.3.2 Continuous-Time Reverse SDE . . . 6
- 2.4 Score Matching and Training Objective . . . 7
  - 2.4.1 Score Matching and Denoising Score Matching . . . 7
- 2.5 Sampling Procedures . . . 8
  - 2.5.1 Reverse SDE Sampling via Euler-Maruyama Method . . . 8
  - 2.5.2 Predictor-Corrector Sampling . . . 8
- 2.6 Noise Schedules . . . 9
  - 2.6.1 Linear Schedules . . . 9
  - 2.6.2 Cosine Variance-Preserving Schedule . . . 9
- 2.7 Summary . . . 10

3 Protein Structure Modelling with Graph Neural Networks **12**
- 3.1 Protein Structure and Motivation . . . 12
- 3.2 Graph Representation of Backbones . . . 13
- 3.3 Score Models Architectures . . . 15
  - 3.3.1 UNet Architecture on Padded Data . . . 15
  - 3.3.2 Graph Neural Network on Graph-Structured Data . . . 15
- 3.4 Summary . . . 17

4 Experiments **18**
- 4.1 Dataset . . . 18
- 4.2 Training and Sampling . . . 18
- 4.3 Evaluation Metrics . . . 18
- 4.4 Quantitative Results . . . 19
- 4.5 Qualitative Visualisation . . . 22
- 4.6 Summary of Results . . . 22

5 Discussion and Conclusion **24**
- 5.1 Discussion of Results . . . 24
- 5.2 Limitations . . . 24
- 5.3 Future Work . . . 24

5.4 Conclusion 25

A Code Appendix **26**

List of Figures

1 Linear schedule vs. cosine schedule. 10
2 Schematic diagram of an amino acid and polypeptide chain from Branden and Tooze (2012). In this dissertation, we are interested only in the backbone formed by C_α atoms. 12
3 Distribution and box plot of RMSD values across test structures. Lower is better. 20
4 Distribution and box plot of TM-scores across test structures. Higher is better. 21
5 RMSD and TM-score versus backbone length L. 21
6 PyMOL visualisation of generated backbone samples from different models 23

List of Tables

1 Summary statistics of backbone lengths in the CATH S40 dataset. 18
2 Quantitative evaluation of backbone reconstruction fidelity. Values reported are mean ± standard deviation. 20

1 Introduction

1.1 Background on Diffusion Models

Diffusion models have recently emerged as one of the most powerful classes of deep generative models, achieving state-of-the-art performance in a wide range of domains, most prominently in image generation Ho et al. (2020); Dhariwal and Nichol (2021). These models construct a forward process that gradually corrupts data with Gaussian noise and train a neural network to approximate the reverse-time dynamics that iteratively remove noise. The resulting generative process is both probabilistically principled and empirically effective, offering advantages in sample quality and training stability compared to earlier paradigms such as variational autoencoders (VAEs) Kingma and Welling (2022) and generative adversarial networks (GANs) Goodfellow et al. (2020).

Score-based diffusion models Song et al. (2021b,a) improve discrete-time denoising diffusion probabilistic models with continuous-time stochastic differential equations (SDEs). Instead of directly parameterising the reverse process, they learn the score function—the gradient of the log-density of the noisy distribution—which enables the use of a variety of forward SDEs and corresponding reverse-time samplers. This framework has proven highly flexible and has been successfully applied to domains including image generation, audio synthesis, point clouds, and molecular data.

1.2 Motivation: Protein Structure Generation

Proteins are essential macromolecules whose biological functions are determined by their three-dimensional structures. The ability to generate novel protein structures has immense implications for biomedical science, including de novo protein design, drug discovery, and enzyme engineering. However, protein structures are highly constrained: bond lengths and angles must remain within narrow physical ranges, torsional angles follow characteristic distributions, and valid folds must satisfy global topological requirements. These constraints make the generative task significantly more challenging than in image or text domains.

Recent advances in deep learning, most notably AlphaFold Jumper et al. (2021), have demonstrated the power of data-driven models in predicting native structures from sequence. Yet, the problem of generating realistic, diverse backbones without explicit sequence conditioning remains an open challenge.

1.3 Diffusion Models for Protein Structures

The probabilistic formulation of score-based diffusion models makes them a natural candidate for modelling protein structures. Unlike GANs, diffusion models provide a likelihood-based framework, and unlike VAEs, they avoid restrictive parametric assumptions about the latent space. Moreover, their iterative denoising dynamics align well with the notion of refining approximate structures toward physically plausible conformations.

Recent work has demonstrated the potential of diffusion-based approaches in protein modelling and design. For example, RFdiffusion Watson et al. (2023) introduced a powerful

framework for de novo protein design, achieving unprecedented results in generating novel folds and functional structures. FoldingDiff Wu et al. (2024) proposed a diffusion-based model that explicitly learns the folding process, while DiffDock Yim et al. (2024) applied diffusion models to protein-ligand docking, highlighting the versatility of the paradigm in structural biology. These developments underscore the promise of diffusion generative models in capturing the rich geometric and biophysical constraints inherent to protein structures.

Applying diffusion models to proteins requires careful representation choices. In this work, we consider the protein backbone as a graph where nodes correspond to Cα atoms and edges encode both spatial proximity and sequential adjacency. This enables the use of graph neural networks (GNNs) Scarselli et al. (2009) as score models, incorporating geometric information through radial basis encodings, directional vectors, and positional embeddings. By training such models on large structural datasets, it becomes possible to learn score functions over protein conformational space and to generate new backbone structures through reverse diffusion.

1.4 Structure of the Dissertation

Section 2 presents the theoretical foundations of score-based diffusion, the representation of protein backbones, and the model architectures explored. Section 4 describes the experimental setup, training procedure, and evaluation metrics, and reports quantitative and qualitative results. And discusses the implications of our findings, limitations, and avenues for future research. Section 5 concludes the dissertation by summarising contributions and highlighting potential future directions.

2 Score-Based Diffusion for Generative Modelling

2.1 Background and Motivation

Generative modelling aims to learn a distribution from which new samples can be drawn that resemble those observed in a dataset. Classical approaches include variational autoencoders (VAEs) (Kingma and Welling, 2022), which maximise a variational lower bound on the likelihood, and generative adversarial networks (GANs) (Goodfellow et al., 2020), which frame generation as an adversarial game. While each of these paradigms has been successful, they also suffer from characteristic drawbacks such as blurry reconstructions (VAEs) and mode collapse (GANs).

Diffusion models represent a more recent class of generative models that address many of these limitations. The central idea is deceptively simple: one defines a forward process that gradually corrupts data with noise until the signal is destroyed, and then learns a reverse process that reconstructs data from noise. By formulating the forward process as a diffusion and training a neural network to approximate the reverse dynamics, diffusion models combine the flexibility of deep networks with the probabilistic rigour of latent-variable models.

In their original formulation, denoising diffusion probabilistic models (DDPMs) (Ho et al., 2020) defined the forward process as a discrete-time Gaussian Markov chain. Subsequent work by Song et al. (2021b) showed that diffusion models can be generalised to continuous-time stochastic differential equations (SDEs). In this framework, the key object is the score function, i.e. the gradient of the log-density of the noisy distribution. Learning this score function allows one to simulate the reverse SDE and thereby generate new samples.

This chapter develops the theoretical foundations of score-based diffusion models in detail. We begin with the definition of the forward diffusion process, proceed to the derivation of the reverse-time dynamics, introduce score matching as the training objective, and describe practical sampling algorithms and noise schedules. Together, these elements form the mathematical basis for applying diffusion models to protein backbone generation in later chapters.

2.2 Forward Diffusion Processes

The first component of a diffusion generative model is the forward, or noising, process. This process gradually perturbs the data distribution into a tractable prior distribution, typically a standard Gaussian. The key requirement is that this transformation be both easy to sample from and analytically tractable, so that training objectives can be computed efficiently.

2.2.1 Discrete-Time Formulation

Denote clean data samples by $x_0 \sim p_{\text{data}}(x)$. Denoising diffusion probabilistic models (DDPMs) (Ho et al., 2020) define the forward process as a Markov chain of N steps:

$$q\left(x_{1:N} \mid x_0\right) \coloneqq \prod_{i=1}^{N} q\left(x_i | x_{i-1}\right),$$

where each transition adds a small amount of Gaussian noise,

$$q\left(x_i \mid x_{i-1}\right) \coloneqq \mathcal{N}\Big(x_i; \sqrt{1-\beta_i}\, x_{i-1},\, \beta_i I\Big), \quad i = 1, ..., N. \tag{1}$$

This produces a sequence of progressively noisier variables $\{x_i\}_{i=1}^N$. Here, $\{\beta_i\}_{i=1}^N$ is a variance schedule with $\beta_i \in (0, 1)$ controlling the noise injected at each step.

A key property of the Gaussian forward process is that one can sample x_t at any arbitrary time step directly from the data x_0:

$$q\left(x_i \mid x_0\right) = \mathcal{N}\Big(x_i; \sqrt{\bar{\alpha}_i}\, x_0,\, (1-\bar{\alpha}_i) I\Big), \tag{2}$$

where $\alpha_i = 1 - \beta_i$ and $\bar{\alpha}_i = \prod_{s=1}^{i} \alpha_s$. This closed form is crucial for training, as it allows drawing noisy samples x_t without explicitly simulating all intermediate steps.

2.2.2 Continuous-Time Formulation

Song et al. (2021b) generalised the discrete diffusion process to continuous time by taking the limit as $N \to \infty$ and $\beta_i \to 0$. In this setting, the forward process can be expressed as a stochastic differential equation (SDE) of the form

$$dx = f(x, t)\, dt + g(t)\, dw, \tag{3}$$

where w is the Brownian motion, $f(x, t)$ is a drift term, and $g(t)$ controls the diffusion magnitude. The SDE produces a trajectory of continuously noisier variables $\{x(t)\}_{t\in[0,T]}$.

For DDPM Gaussian transition kernel eq. (1), the chain is equivalent to

$$x_i = \sqrt{1-\beta_i}\, x_{i-1} + \sqrt{\beta_i}\, z_{i-1}, \quad i = 1, ..., N,$$

where $z_{i-1} \sim \mathcal{N}(0, I)$. Define functions $\beta\left(\frac{i}{N}\right) \coloneqq N\beta_i$, $x\left(\frac{i}{N}\right) = x_i$ and $z\left(\frac{i}{N}\right) = z_i$, stepsize $\Delta t \coloneqq 1/N$ and finally reparameterise the time as $t = i\Delta t \in \{0, \Delta t, ..., N\Delta t = 1\}$, we have

$$\begin{aligned} x(t) &= \sqrt{1-\beta(t)\,\Delta t}\, x(t-\Delta t) + \sqrt{\beta(t)\,\Delta t}\, z\left(t-\Delta t\right) \\ &\overset{\Delta t \ll 1}{\approx} \left(1 - \frac{1}{2}\beta(t)\,\Delta t\right) x(t-\Delta t) + \sqrt{\beta(t)\,\Delta t}\, z\left(t-\Delta t\right), \end{aligned}$$

that is

$$x(t) - x(t-\Delta t) = -\frac{1}{2}\beta(t)\,\Delta t x(t-\Delta t) + \sqrt{\beta(t)\,\Delta t}\, z\left(t-\Delta t\right).$$

In the limit of $\Delta t \to 0$, the above equation converges to

$$dx = -\frac{1}{2}\beta(t)\,x dt + \sqrt{\beta(t)}dw. \tag{4}$$

Equation (4) is refered to as the Variance-preserving (VP) SDE, where $\beta(t)$ is the noise schedule (e.g. linear, cosine). Just like the discrete case of DDPM, VP SDE has a closed form solution. Define

$$u\left(x(t), t\right) = \exp\left(\frac{1}{2}\int_0^t \beta(s)\,ds\right) x(t)\,.$$

Then by Itô's chain rule, $y(t) \coloneqq u\left(x(t), t\right)$ has the SDE

$$\begin{aligned} dy &= \frac{1}{2}\beta(t)\exp\left(\frac{1}{2}\int_0^t \beta(s)\,ds\right) x(t)\,dt + \exp\left(\frac{1}{2}\int_0^t \beta(s)\,ds\right) dx \\ &= \exp\left(\frac{1}{2}\int_0^t \beta(s)\,ds\right)\left(\frac{1}{2}\beta(t)\,x(t)\,dt - \frac{1}{2}\beta(t)\,x(t)\,dt + \sqrt{\beta(t)}dw\right) \\ &= \exp\left(\frac{1}{2}\int_0^t \beta(s)\,ds\right)\sqrt{\beta(t)}dw. \end{aligned}$$

Integrate from 0 to t yields

$$y(t) = y(0) + \int_0^t \exp\left(\frac{1}{2}\int_0^s \beta(u)\,du\right)\sqrt{\beta(s)}dw_s.$$

Now undo the change of variables we have

$$\begin{aligned} x(t) &= \left[\exp\left(\frac{1}{2}\int_0^t \beta(s)\,ds\right)\right]^{-1} y(t) \\ &= \exp\left(-\frac{1}{2}\int_0^t \beta(s)\,ds\right)x(0) + \int_0^t \exp\left(-\frac{1}{2}\int_s^t \beta(u)\,du\right)\sqrt{\beta(s)}dw_s. \end{aligned}$$

The initial condition $x(0) = x_0$ is a sample from dataset, i.e., a constant, so the posterior of perturbation (or the prior of the reverse sampling) is a Gaussian distribution with mean

$$\mathbb{E}\left[x(t) \mid x(0) = x_0\right] = \exp\left(-\frac{1}{2}\int_0^t \beta(s)\,ds\right)x_0 \tag{5}$$

and variance

$$\begin{aligned} \mathrm{Var}\left[x(t) \mid x(0) = x_0\right] &= \int_0^t \exp\left(-\int_s^t \beta(u)\,du\right)\beta(s)\,ds I \\ &= \left(1 - \exp\left(-\int_0^t \beta(s)\,ds\right)\right) I \end{aligned} \tag{6}$$

that is

$$p(x_t|x_0) = \mathcal{N}\left(x_t :\ x_0 e^{-\frac{1}{2}\int_0^t \beta(s)ds}, \left(1 - e^{-\int_0^t \beta(s)ds}\right) I\right). \tag{7}$$

Obviously the variance is always bounded, hence the name variance-preserving. This continuous formulation provides a flexible mathematical foundation that unifies discrete DDPMs with stochastic differential equations, and it allows the use of stochastic calculus tools to analyse and manipulate diffusion models. In particular, it enables the derivation of the reverse-time SDE, which defines the generative process and will be introduced in the next section.

Other choices of f and g in eq. (3) yield different diffusion processes, Song et al. (2021b) shown three categories,

- **Variance-preserving (VP) SDE**: maintains the marginal variance of x_t at one throughout the process.
- **Variance-exploding (VE) SDE**: variance grows unbounded as $t \to T$, pushing the distribution to white noise.
- **Sub-variance-preserving (sub-VP) SDE**: an interpolation between VP and VE.

We will focus on VP SDE in this dissertation.

2.3 Reverse-Time Diffusion Processes

The forward diffusion process, whether in discrete or continuous form, progressively perturbs data until its distribution approaches a simple prior such as an isotropic Gaussian. To perform generative modelling, we require a process that inverts this corruption: starting from noise and evolving back toward the data distribution. This is formalised through the theory of time-reversal for diffusion processes.

2.3.1 Discrete-Time Reverse Process

In the discrete DDPM formulation Ho et al. (2020), the generative model is defined as a reverse Markov chain

$$p_\theta\left(x_{0:N}\right) \coloneqq p(x_N) \prod_{i=1}^{N} p_\theta(x_{i-1} \mid x_i),$$

with $p(x_N) = \mathcal{N}(x_N; 0, I)$ as the prior. The reverse conditionals are modelled as Gaussians

$$p_\theta\left(x_{i-1} \mid x_t\right) \coloneqq \mathcal{N}\big(x_{i-1}; \mu_\theta(x_i, i), \Sigma_\theta(x_i, i)\big),$$

where μ_θ and Σ_θ are learned using a neural network with parameter θ. Training then consists of minimising the Kullback-Leibler divergence between the true posterior $q(x_{i-1} \mid x_i, x_0)$ and the model distribution $p_\theta(x_{i-1} \mid x_i)$.

2.3.2 Continuous-Time Reverse SDE

In the continuous-time setting, Anderson (1982) established that the time reversal of an Itô SDE (3) is itself an SDE with modified drift term,

$$dx = \left[f(x,t) - g^2(t)\nabla_x \log p_t(x)\right]\, dt + g(t)\, d\bar{w}, \tag{8}$$

where $\bar{w}$ is the Brownian motion running backward in time, $\nabla_x \log p_t(x)$ is the score function at time t, that is, the gradient of the log-density of the perturbed, marginal, data distribution $p_t(x)$. This equation defines the reverse-time SDE. It depends explicitly on the score function $\nabla_x \log p_t(x)$ of the forward process marginal distribution $p_t(x)$.

For VP SDE eq. (4), the reverse-time SDE is given by

$$dx = \left[-\frac{1}{2}\beta(t)\, x - \beta(t)\, \nabla_x \log p_t(x)\right] dt + \sqrt{\beta(t)} d\bar{w}.$$

Though it has no closed form sulution, if one can estimate the score function accurately for all times t, it becomes possible to simulate the reverse SDE and generate samples from the data distribution.

This result provides the key insight underlying score-based diffusion: generative modelling reduces to score estimation. Rather than directly modelling likelihoods or sampling distributions, we train a neural network $s_\theta(x, t)$ to approximate the score $\nabla_x \log p_t(x)$. The network is then used to guide the drift of the reverse SDE, producing realistic samples when integrated from Gaussian noise at $t = 1$ back to $t = 0$.

2.4 Score Matching and Training Objective

The reverse-time SDE depends on the score function $\nabla_x \log p_t(x)$, which is generally intractable. Thus, the central learning problem in score-based diffusion is to approximate this score with a neural network $s_\theta(x, t)$, called time dependent score network (TDSN) (Song et al., 2021b). Training requires a loss function that encourages s_θ to match the true score across noise levels.

2.4.1 Score Matching and Denoising Score Matching

For each time t, the score function of x_t can be trained via minimising the Fisher divergence

$$\mathbb{E}_{p(x_t)}\left[\left\|\nabla_{x_t} \log p\left(x_t\right) - s_\theta\left(x_t, t\right)\right\|_2^2\right].$$

The unknown term $\nabla_{x_t} \log p\left(x_t\right)$ (true score) can be eliminated with the score matching objective Hyvärinen (2005)

$$J_t^{\mathrm{SM}}(\theta) = \mathbb{E}_{p(x_t)}\left[\left\|\mathrm{tr}\left(\nabla_{x_t} s_\theta\left(x_t, t\right)\right) - \frac{1}{2}\|s_\theta(x_t, t)\|_2^2\right\|_2^2\right].$$

Note that the term $\mathrm{tr}\left(\nabla_{x_t} s_\theta\left(x_t, t\right)\right)$ can be computationally intensive. Vincent (2011) showed that training a denoising autoencoder to reconstruct clean data from corrupted observations is equivalent to score matching under certain conditions. This connection underpins the training of diffusion models: the neural network is trained to denoise x_t into x_0, thereby learning the score function implicitly. Hence, in the case of VP SDE, since we have the analytic form of the posterior, eq. (7), the denoising score matching objective is given by

$$J_t^{\mathrm{DSM}} = \mathbb{E}_{x_0 \sim p_{\mathrm{data}}(x_0)} \mathbb{E}_{x_t \sim p(x_t|x_0)}\left[\left\|s_\theta\left(x_t, t\right) - \nabla_{x_t} \log p\left(x_t|x_0\right)\right\|_2^2\right]$$

$$= \mathbb{E}_{x_0 \sim p_{\text{data}}(x_0)} \mathbb{E}_{x_t \sim p(x_t|x_0)} \left[\left\| s_\theta\left(x_t, t\right) + \frac{x_t - \mu_t}{\sigma_t^2} \right\|_2^2 \right]$$

where μ_t and σ_t^2 are given by eqs. (5) and (6), respectively.

The denoising score matching objective J_t^{DSM} is for a specific time t. To train the score model across all time $t \in [0, 1]$ in one go, the overall objective is given by a weighted sum (or average) (Song et al., 2021b)

$$J^{\text{DSM}} = \mathbb{E}_{t \sim \mathcal{U}(0,1)} \left[\lambda(t)\, J_t^{\text{DSM}} \right], \tag{9}$$

where $\lambda(t)$ is a positive weighting function.

The learning problem for score-based diffusion therefore reduces to denoising score matching: the neural network $s_\theta(x, t)$ is trained to approximate $\nabla_x \log p_t(x)$ across different noise levels. Once trained, this network can be used to drive the reverse SDE, enabling generation of new samples from Gaussian noise.

2.5 Sampling Procedures

Once the score network $s_\theta(x, t)$ has been trained, new samples can be generated by simulating the reverse diffusion process. This requires integrating the reverse-time SDE (8) starting from Gaussian noise $x(t = 1) \sim \mathcal{N}(0, I)$ and evolving toward $t = 0$.

2.5.1 Reverse SDE Sampling via Euler-Maruyama Method

The simplest approach is to discretise the reverse SDE using the Euler-Maruyama method. For a decreasing sequence of time steps $\{t_i\}_{i=0}^N$ with $t_N = 1$ and $t_0 = 0$, the update rule is

$$x_{t_{i-1}} = x_{t_i} + \left[f(x_{t_i}, t_i) - g(t_i)^2 s_\theta(x_{t_i}, t_i) \right] \Delta t + g(t_i) \sqrt{\Delta t}\, z_i, \tag{10}$$

where $z_i \sim \mathcal{N}(0, I)$ and $\Delta t = t_{i-1} - t_i$. This procedure generates approximate samples from the data distribution. While straightforward, its quality depends heavily on the number of discretisation steps: smaller steps yield higher fidelity at the cost of computational time.

2.5.2 Predictor-Corrector Sampling

The Predictor-Corrector sampler was proposed by Song et al. (2021b) as an improved sampling method. It is based on combining two components:

1. **Predictor step:** one update using the reverse SDE (e.g., via Euler-Maruyama method, eq. (10)), advancing the trajectory toward lower noise levels.
2. **Corrector step:** one or more steps of stochastic refinement, implemented as Langevin Monte Carlo:

   $$x \leftarrow x + \epsilon\, s_\theta(x, t) + \sqrt{2\epsilon}\, z, \quad z \sim \mathcal{N}(0, I),$$

   where ϵ is a step size. This step locally improves sample quality by pushing the state toward regions of higher density according to the trained score network.

By alternating predictor and corrector steps, the algorithm achieves a better trade-off between quality and efficiency than pure reverse SDE sampling. In practice, only a few corrector iterations per time step are needed to significantly improve sample fidelity.

In this dissertation, we use predictor-corrector sampling as our default procedure.

2.6 Noise Schedules

The design of the noise schedule plays a central role in the performance of score-based diffusion models. The schedule determines how the variance of the forward diffusion process evolves over time, which directly influences both training stability and the quality of generated samples.

2.6.1 Linear Schedules

In the original DDPM formulation (Ho et al., 2020), the variance schedule $\{\beta_i\}_{i=1}^N$ was chosen to increase linearly from a small value to a larger one over N steps. Equivalently, in the continuous SDE formulation (Song et al., 2021b), this corresponds to a linear growth of the noise rate

$$\beta(t) = \beta_0 + (\beta_1 - \beta_0)\, t.$$

While simple, this schedule can be suboptimal: early time steps may inject too little noise, leading to poor coverage of high-noise regions during training, while later steps may over-noise the data, resulting in wasted computation.

2.6.2 Cosine Variance-Preserving Schedule

Nichol and Dhariwal (2021) proposed a cosine schedule for the noising process in DDPM, which has since become widely adopted (Dhariwal and Nichol, 2021; Saharia et al., 2022; Watson et al., 2023). The proposed cosine schedule corresponds to using

$$\bar{\alpha}_i = \frac{\cos^2\left(\frac{\pi}{2} \cdot \frac{i/N+s}{1+s}\right)}{\cos^2\left(\frac{\pi}{2}\frac{s}{1+s}\right)}$$

in eq. (2) for noising process, where s is a very small offset (typically 10^{-4}) to prevent singularities, that is (ignoring the denominator in $\bar{\alpha}_i$ as it is nearly 1 for small s),

$$x_i = \sqrt{\bar{\alpha}_i}\, x_0 + \sqrt{1-\bar{\alpha}_i}\, z_i, \quad \bar{\alpha}_i \approx \cos^2\left(\frac{\pi}{2} \cdot \frac{i/N+s}{1+s}\right), \quad z_i \sim \mathcal{N}(0, I)\,.$$

This is a DDPM perturbation scheme. To generalise to continuous time, we do exactly the same as in section 2.2.2: define function $\bar{\alpha}\left(\frac{i}{N}\right) \coloneqq \bar{\alpha}_i$, stepsize $\Delta t \coloneqq 1/N$ and time as $t = i\Delta t \in \{0, \Delta t, ..., N\Delta t = 1\}$. This yields the continuous time schedule

$$x(t) = \sqrt{\bar{\alpha}(t)}\, x(0) + \sqrt{1-\bar{\alpha}(t)}\, z(t)\,, \quad \bar{\alpha}(t) = \cos^2\left(\frac{\pi}{2} \cdot \frac{t+s}{1+s}\right), \quad z(t) \sim \mathcal{N}(0, I)\,.$$

Match with previous derivation, eq. (7), we are left to solve

$$\bar{\alpha}(t) = e^{-\int_0^t \beta(s)ds}.$$

It follows that

$$\begin{aligned}
\beta(t) &= -\frac{d}{dt}\log\cos^2\left(\frac{\pi}{2}\cdot\frac{t+s}{1+s}\right) \\
&= -\frac{1}{\cos^2\left(\frac{\pi}{2}\cdot\frac{t+s}{1+s}\right)}\left[2\cos\left(\frac{\pi}{2}\cdot\frac{t+s}{1+s}\right)\right]\left[-\sin\left(\frac{\pi}{2}\cdot\frac{t+s}{1+s}\right)\right]\frac{d}{dt}\left(\frac{\pi}{2}\cdot\frac{t+s}{1+s}\right) \\
&= \frac{\pi}{1+s}\tan\left(\frac{\pi}{2}\cdot\frac{t+s}{1+s}\right). \qquad (11)
\end{aligned}$$

Instead of linear growth, the cosine schedule ensures a smoother increase in noise variance, the noising strength changes much slower near $i = 1$ and $i = N$, as illustrated by fig. 1. This schedule maintains higher signal levels for longer, enabling the score network to learn more effectively across a wider range of noise intensities.

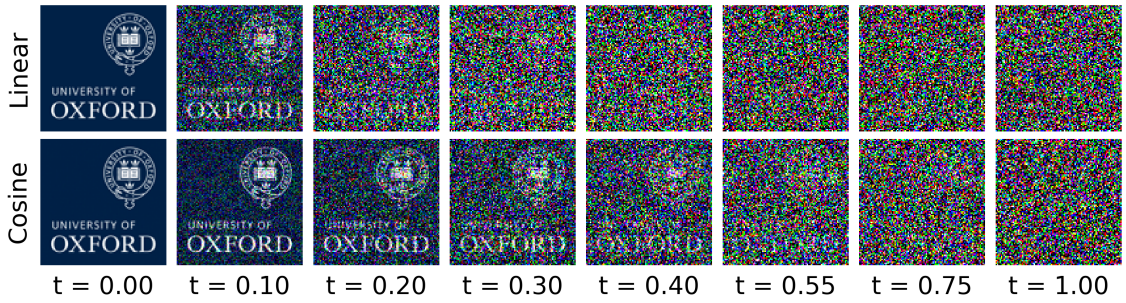

Figure 1: Linear schedule vs. cosine schedule.

Empirically, the cosine schedule improves sample quality and accelerates convergence compared to linear schedules. It balances the trade-off between injecting sufficient noise for diversity and preserving enough signal for stable training. Moreover, because it avoids excessively noisy late stages, fewer discretisation steps are needed during sampling, reducing computational cost.

In this dissertation, we adopt this cosine schedule as the forward diffusion process. This choice is motivated by its demonstrated effectiveness in image and structural generative tasks (Dhariwal and Nichol, 2021; Saharia et al., 2022; Watson et al., 2023), and by its compatibility with the variance-preserving SDE formulation used in our score model, eq. (11). All experiments in later chapters therefore use the cosine schedule as the default setting.

2.7 Summary

This chapter has established the theoretical foundations of score-based diffusion models, which form the core generative framework employed in this dissertation. We began by introducing the forward diffusion process, first in its discrete DDPM formulation and then in its continuous-time generalisation as a stochastic differential equation. We then

derived the reverse-time SDE, showing that generative modelling reduces to the problem of score estimation. This led naturally to the denoising score matching objective, which enables training a neural network to approximate the score function across all noise levels. Finally, we discussed practical sampling algorithms, including reverse SDE integration and predictor-corrector methods, and examined the role of noise schedules, with particular emphasis on the cosine variance-preserving schedule adopted in this work.

Together, these elements provide a principled probabilistic framework for deep generative modelling. Unlike GANs or VAEs, score-based diffusion models avoid common issues such as mode collapse or restrictive latent assumptions, while offering strong theoretical guarantees and flexible sampling procedures. The remainder of this dissertation builds upon these foundations to adapt score-based diffusion to the setting of protein backbone generation, where structural constraints and geometric representations introduce unique modelling challenges.

3 Protein Structure Modelling with Graph Neural Networks

3.1 Protein Structure and Motivation

Proteins are built from amino acids, small organic molecules that share a common structure: a central alpha carbon (C_α) bonded to an amino group, a carboxyl group, a hydrogen atom, and a variable side chain. Amino acids are joined linearly by peptide bonds, which link the amino group of one amino acid to the carboxyl group of the next, forming a polypeptide chain. The sequence of amino acids in this chain defines the primary structure of a protein, while the chemistry of their side chains drives folding into higher-order structures (Creighton, 1993; Branden and Tooze, 2012). Understanding and modelling protein structures is a central challenge in computational biology because structure underlies stability, dynamics, and molecular interactions.

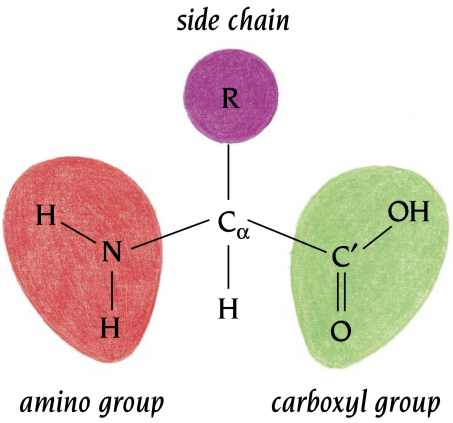

(a) Amino acid

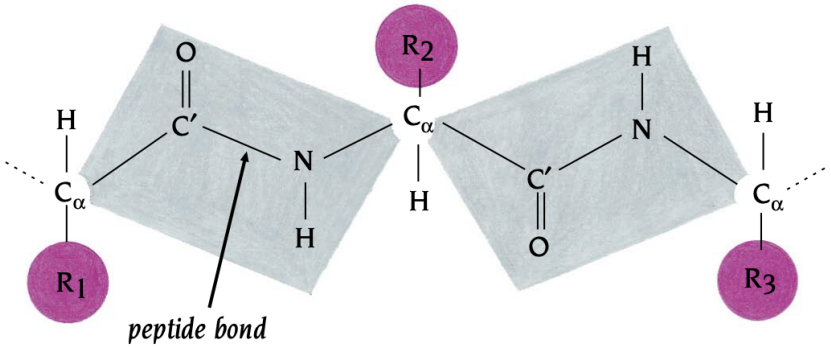

(b) Polypeptide chain

Figure 2: Schematic diagram of an amino acid and polypeptide chain from Branden and Tooze (2012). In this dissertation, we are interested only in the backbone formed by C_α atoms.

Because the C_α atoms define the backbone geometry of the chain, they provide a natural coarse-grained representation for structural modelling. In this work we adopt a C_α-only representation: for a protein (chain of amino acid) x of length L, each amino acid

$i \in \{1, \ldots, L\}$ is associated with a 3D coordinate $x^i \in \mathbb{R}^3$, so $x \in \mathbb{R}^{L\times 3}$. This coarse-grained representation is widely used in structural modelling because it captures global fold geometry and secondary structure while keeping the state space compact, making it well-suited to generative modelling (Watson et al., 2023; Zhang and Skolnick, 2005; Senior et al., 2020).

Even at this simplified level, protein geometry is far from arbitrary. The distance between successive C_α atoms is consistently about

$$\|x^i - x^{i-1}\| \approx 3.8 \text{ Å}.$$

Local backbone conformation can be described by the angle formed by three consecutive C_α atoms, $\angle(x^{i-1}, x^i, x^{i+1})$, and by the dihedral angle defined by four consecutive C_α atoms, $\text{dihedral}(x^{i-2}, x^{i-1}, x^i, x^{i+1})$. The empirically observed distributions of these geometric quantities are restricted by steric hindrance and the planarity of the peptide bond. Beyond these local constraints, valid structures must also avoid steric clashes, where non-adjacent amino acids are placed unrealistically close in space, and they typically fold into compact, physically plausible conformations (Creighton, 1993; Branden and Tooze, 2012).

These intricate three-dimensional dependencies make protein backbones fundamentally different from unstructured data such as images or text. Consequently, generative models for proteins must account for spatial and structural constraints explicitly, motivating the use of geometry-aware representations and neural architectures.

Scope of this work. Our goal is backbone-level generative modelling using score-based diffusion. We do not impose hard geometric constraints during training or sampling (e.g. fixed bond lengths or bond angles); instead, we learn the distribution over C_α coordinate trajectories and evaluate fidelity against native backbones. Section 4 reports RMSD/TM results and discusses the limitation that high RMSD or low TM can still correspond to physically valid but non-native folds.

3.2 Graph Representation of Backbones

A protein backbone of length L is represented as a graph $G = (V, E)$, where each amino acid (or its corresponding C_α atoms) corresponds to a node and edges capture both geometric proximity and sequential connectivity. This formulation enables the use of graph neural networks as score models, allowing information to be propagated through local neighbourhoods while respecting the spatial structure of the backbone.

Nodes and node features. Each node $i \in V$ corresponds to a amino acid with coordinate $x^i \in \mathbb{R}^3$ representing the position of its C_α atom. For simplicity, we do not include amino acid type or side-chain information in this work, focusing purely on the geometry of the C_α atoms backbone. In addition to the coordinates (perturbation noises), extra node features are initialised as positional embeddings derived from the amino acid index (see section 3.3, eq. (14)), along with time-conditioning features from the diffusion process (see section 3.3, eq. (13)). The full node feature vector is then obtained by concatenation:

$$\text{Node feature} = \big[\ \text{noises} \parallel \text{positional embedding} \parallel \text{time embedding}\ \big].$$

Edges. Edges are constructed using a radius graph: for each node $i \in V$, we connect edges to all neighbours j within a cutoff distance r, subject to a maximum of k nearest neighbours. Formally,

$$(i, j) \in E \quad \Leftrightarrow \quad \|x^i - x^j\| \leq r \quad \text{and} \quad j \text{ is among the } k \text{ closest to } i.$$

This design ensures that local spatial relationships are captured without requiring a fixed sequence length. In addition to geometric edges, self-loops are included to stabilise message passing and allow each node to retain its own features. Edges are directed: for each $(i, j) \in E$, messages are passed from j (target) to i (source). This convention is consistent with the implementation in PyTorch Geometric, and we do not duplicate edges to create an undirected graph.

Edge features. For each edge $(i, j) \in E$, we compute a feature vector combining geometric and diffusion-time information. The feature vector includes the following:

- **Radial basis encoding:** The distance $\|x^i - x^j\|$ is expanded into a vector of length M using Gaussian radial basis functions,

$$\phi_\ell(\|x^i - x^j\|) = \exp\left(-\frac{(\|x^i - x^j\| - c_\ell)^2}{2\epsilon^2}\right), \quad \ell = 1, ..., M,$$

  where centres $\{c_\ell\}_{\ell=1}^M$ are distributed uniformly between 0 and cutoff distance r, length scale $\epsilon = r/M$. This provides a smooth representation of distances. It is implemented via `e3nn.soft_one_hot_linspace` from Geiger and Smidt (2022); Geiger et al. (2025).

- **Directional encoding:** The normalised vector

$$d^{(i,j)} = \frac{x^i - x^j}{\|x^i - x^j\|} \in \mathbb{R}^3$$

  encodes the relative orientation of the neighbour. This directional feature allows the network to capture local geometry beyond mere distances (Watson et al., 2023).

- **Time embedding:** The diffusion timestep t is embedded into high-dimensional features (see section 3.3, eq. (13)) and projected through a linear layer. For each edge (i, j), we associate the time embedding with the source node i, enabling time-dependent conditioning of messages.

The full edge feature vector is then obtained by concatenation:

$$h_{ij} = \left[\phi_{1:M} \parallel d^{(i,j)}, \forall (i, j) \in E \parallel \text{time embedding} \right].$$

Rationale. This graph construction has several desirable properties: (i) it scales linearly with the number of amino acids (C_α atoms) L, (ii) it incorporates both distance and orientation information, which are critical for protein geometry, and (iii) it enables variable-length backbones to be handled naturally without padding. These features make it well-suited for score-based diffusion over protein structures.

3.3 Score Models Architectures

The score network $s_\theta(x, t)$ is parameterised by a neural network that maps noisy protein backbones to score estimates. We explore several architectures of increasing complexity, from a padding-based UNet model to a Graph Neural Network that utilises the graph representation.

3.3.1 UNet Architecture on Padded Data

As a baseline, we implemented a UNet architecture (Ronneberger et al., 2015) with one dimensional convolutional neural networks applied directly to backbone coordinates represented as sequences of fixed length. Each protein was zero-padded to a common maximum length, and the UNet operated on the resulting coordinate tensors. This design provides a simple convolutional benchmark but does not handle variable-length inputs naturally and discards explicit geometric relationships between amino acids. It serves primarily as a sanity check to compare graph-based approaches against a conventional deep learning model.

3.3.2 Graph Neural Network on Graph-Structured Data

Graph Neural Networks. Convolutional layers on graph-structured data can be implemented via Graph Neural Networks (GNNs) (Scarselli et al., 2009; Gilmer et al., 2017; Kipf and Welling, 2017; Battaglia et al., 2018), which extend the idea of neural networks to arbitrary graph domains. In this framework, each node updates its representation by aggregating information, or messages, from its neighbours, typically following the generic message passing scheme (Gilmer et al., 2017)

$$h_i^{(\ell+1)} \;=\; U\Big(h_i^{(\ell)},\; M(\mathcal{N}(i))\Big)\,, \tag{12}$$

where $h_i^{(\ell)}$ is the hidden state of node i at layer ℓ, $\mathcal{N}(i)$ denotes the neighbourhood of node i, M is a function that computes messages from the features of neighbouring nodes and edges, and U is an update function that integrates these messages into the node state.

Various graph neural network architectures are available in the PyTorch Geometric package (Fey and Lenssen, 2019; Fey et al., 2025). In this work we build on the Transformer-based graph convolution network (GCN) (`torch_geometric.nn.conv.TransformerConv`) proposed by Shi et al. (2021), which improves the expressiveness of message passing by incorporating an attention mechanism over both node and edge features. Here the functions M and U in eq. (12) are defined via

$$\begin{aligned} q_i &= W_q h_i^{(\ell)}, \quad k_j = W_k h_j^{(\ell)}, \\ \alpha_{ij}^{(\ell)} &= \mathrm{softmax}_{j\in\mathcal{N}(i)}\big(q_i^\top (k_j + W_e e_{ij})\big), \\ h_i^{(\ell+1)} &= \sum_{j\in\mathcal{N}(i)} \alpha_{ij}^{(\ell)}\, W_v h_j^{(\ell)}, \end{aligned}$$

where e_{ij} is the edge feature vector, $\alpha_{ij}^{(\ell)}$ are the attention weights, and W_q, W_k, W_e, W_v are learnable projections. In practice, multiple attention heads are computed in parallel

and concatenated, but we present the single-head formulation for clarity. This formulation allows geometric encodings such as distances, orientations, and diffusion time embeddings to directly influence the attention weights, making the layer particularly well suited to protein backbone graphs.

Time conditioning via Gaussian Fourier features. Following Song et al. (2021b), we embed the diffusion time step $t \in (0, 1)$ using Gaussian Fourier features (Tancik et al., 2020). Let d_t denote the dimension of time embedding, and let $W \in \mathbb{R}^{d_t/2}$ have independent components $W_k \sim \mathcal{N}(0, s^2)$ for $k = 1, ..., d_t/2$. Then the embedding is defined by

$$\gamma(t) = \left[\cos(2\pi W t),\ \sin(2\pi W t) \right] \in \mathbb{R}^d_t, \tag{13}$$

where cosine and sine are applied elementwise. This provides a smooth and expressive encoding of time, allowing the score network to capture the evolution of noise levels across the diffusion process. In practice, $\gamma(t)$ is passed through a shallow multi-layer perceptron (MLP) before being concatenated with node and edge features to condition the network on the current diffusion step.

Sinusoidal positional embeddings of amino acid indices. Graph-based models are inherently invariant to node permutations, which can be a limitation when modeling protein backbones where the sequential order of amino acids carries biologically meaningful directionality along the chain. To inject this ordering information, each node $i \in \{1, \ldots, L\}$ is assigned a normalized scalar index $i/L \in (0, 1]$. This scalar is mapped to a high-dimensional representation using sinusoidal positional encodings (Vaswani et al., 2017),

$$\rho(i) = \left[\sin(\omega_1 i/L),\ \cos(\omega_1 i/L),\ \ldots,\ \sin(\omega_{d_i/2} i/L),\ \cos(\omega_{d_i/2} i/L) \right] \in \mathbb{R}^{d_i}, \tag{14}$$

where d_i is the dimension of positional embedding, and $\{\omega_k\}$ are fixed, exponentially spaced frequencies. The resulting positional embedding is passed through a shallow multi-layer perceptron (MLP) and concatenated with the initial node features, enabling the network to distinguish amino acids by their sequential position along the backbone.

Residual structure. Training deep graph networks is challenging because repeated aggregation can lead to oversmoothing of node representations and vanishing gradients (Li et al., 2018, 2019). Residual connections (He et al., 2016) have since become a standard component of graph neural networks (Kipf and Welling, 2017; Li et al., 2019). They allow each layer to refine representations relative to the previous ones rather than completely replacing them, facilitating gradient flow through many stacked layers.

In this work we adopt a residual structure for every GNN (`TransformerConv`) block, so that the output of each layer is added to its input before passing through nonlinearities and normalisation. To further stabilise training, we employ GraphNorm (Cai et al., 2021), a normalisation technique specifically designed for graph neural networks. GraphNorm normalises node embeddings using graph-level statistics, improving convergence speed and reducing training instability compared to BatchNorm or LayerNorm.

This combination of residual connections and GraphNorm improves optimisation stability, mitigates oversmoothing, and enables effective training of multi-layer architectures.

Empirically, such designs have been shown to enhance performance on long chains and large graphs, which is particularly important in our setting of protein backbones where sequence lengths vary widely and capturing long-range dependencies is essential.

Remark 3.1. *The UNet baseline provides a simple non-graph benchmark. In practice, the inclusion of positional encodings has a noticeable effect on model quality. To quantify this contribution, we include a second baseline that employs the aforementioned GNN architecture without positional encodings. This variant captures local geometric neighbourhood information but lacks explicit representations of sequential order, thereby limiting its ability to model the directional structure of protein backbones.*

3.4 Summary

In this section we described the methodology for adapting score-based diffusion models to the task of protein backbone generation. We began by outlining the structural constraints of proteins and motivated the use of a C_α-only representation. We then formulated backbones as graphs, with nodes corresponding to amino acids and edges defined through a radius neighbourhood, augmented by radial basis encodings, directional features, and diffusion-time embeddings. This representation captures geometric information in a permutation-invariant manner while naturally supporting variable-length backbones.

We constructed a graph neural network for the score network: a residual Transformer-based GCN with positional embeddings. The latter integrates geometric, sequential, and temporal information, supported by residual connections and GraphNorm.

These methodological components together establish a principled framework for generative modelling of protein backbones using score-based diffusion. The next section presents experimental results, benchmarking these models on the CATH S40 dataset using both quantitative metrics (RMSD, TM-score) and qualitative structural visualisations.

4 Experiments

This section presents the experimental evaluation of the score-based diffusion models described in sections 2 and 3. We benchmark three architectures on the CATH S40 dataset and assess their performance using quantitative metrics and qualitative visualisations.

4.1 Dataset

We train our models on the CATH S40 dataset (Orengo et al., 1997; Waman et al., 2024; Sillitoe et al., 2021; Lewis et al., 2018), a widely used benchmark for structural modelling tasks. The dataset clusters protein domains at 40% sequence identity, ensuring reduced redundancy while maintaining broad structural diversity.

For each protein domain, we extract the backbone coordinates by retaining only the C_α atom of each amino acid, yielding a variable-length sequence of coordinates $\{x^i \in \mathbb{R}^3\}_{i=1}^L$, where L denotes the chain length, as mentioned in section 3.1. The statistics of backbone lengths is summarised in table 1. Backbones are then converted into graphs as described in section 3.2, and coordinates are normalised prior to training.

Table 1: Summary statistics of backbone lengths in the CATH S40 dataset.

	Min	Max	Mean	Median	Std
Length (L)	11	1202	155	133	89

4.2 Training and Sampling

Training setup. For the forward noising process we adopt the variance-preserving (VP) SDE formulation (eq. (4)) with the cosine noise schedule (eq. (11)). The training objective is the denoising score matching loss (eq. (9)), optimising the score networks described in section 3.3. Models are trained using the Adam optimiser (Kingma and Ba, 2017) with a batch size dynamically adapted to GPU memory constraints.

Sampling. New backbone structures are generated by simulating the reverse SDE using predictor-corrector (PC) sampling, starting from Gaussian noise (section 2.5.2). This procedure enables diverse yet structurally plausible backbone generations.

Implementation. All models are implemented in Python using PyTorch and PyTorch Geometric (Fey and Lenssen, 2019; Fey et al., 2025). Experiments were conducted on NVIDIA GPUs with 48GB memory.

4.3 Evaluation Metrics

We evaluate reconstruction fidelity using two widely adopted measures of structural similarity: root-mean-square deviation (RMSD) and TM-score.

Root-mean-square deviation (RMSD). RMSD provides a direct measure of average atomic displacement between two aligned structures. Given a generated backbone $X = \{x_i\}_{i=1}^{L}$ and its reference $Y = \{y_i\}_{i=1}^{L}$, the RMSD is defined as

$$\mathrm{RMSD}(X, Y) \;=\; \sqrt{\frac{1}{L}\sum_{i=1}^{L} \|x_i - y_i\|^2}.$$

Lower values indicate closer correspondence to the reference. Although widely used, RMSD can be overly sensitive to local misalignments, and large deviations in one region may dominate the score even if the overall fold is preserved.

TM-align and TM-score. To complement RMSD, we use TM-score (Zhang and Skolnick, 2004; Xu and Zhang, 2010), a structural similarity measure in $(0, 1]$, computed via the TM-align algorithm (Zhang and Skolnick, 2005). Unlike RMSD, TM-score is less affected by local errors and more reflective of global fold similarity. In practice, TM-align performs a sequence-independent superposition of two protein structures using heuristic dynamic programming, returning both an optimal alignment and the corresponding TM-score. Interpretation of TM-scores follows established conventions: values below 0.2 typically correspond to unrelated structures, while scores above 0.5 generally indicate that two proteins share the same overall fold within SCOP/CATH classification. Thus, TM-score serves as a more robust global measure of structural fidelity and complements RMSD in our evaluation.

Remark 4.1. *Because each generated backbone is compared to its specific native target of the same length L, RMSD and TM-score measure reconstruction fidelity, not absolute physical validity. This is appropriate for our benchmarking setting (paired evaluation), but one should interpret low TM or high RMSD with caution: a generated backbone may still represent a plausible alternative fold while scoring poorly against the chosen reference.*

4.4 Quantitative Results

We benchmarked three model variants: (i) a UNet baseline on padded coordinate sequences, (ii) a Transformer-based graph convolutional network with and without positional encodings, as detailed in section 3.3. Evaluation was performed using RMSD and TM-score, as described in section 4.3.

Overall performance. The summary statistics of overall performance is reported in table 2. From the results, the Transformer-based graph convolutional network with positional encodings achieves the best overall performance, with the lowest RMSD (16.39 ± 4.29 Å) and highest TM-score (0.272 ± 0.041). By contrast, the same architecture without positional encodings performs substantially worse, highlighting the importance of incorporating sequential information in addition to geometric neighbourhoods. Interestingly, the UNet baseline outperforms the GCN without positional encodings, despite its simplistic design and reliance on padded sequences. This suggests that while graph representations capture local geometry, they require positional encodings to effectively model the directional structure of protein backbones.

Table 2: Quantitative evaluation of backbone reconstruction fidelity. Values reported are mean ± standard deviation.

Model	RMSD (Å)	TM-score
UNet baseline	17.230 ± 4.699	0.264 ± 0.041
GCN w/o positional encoding	20.459 ± 4.985	0.145 ± 0.023
GCN w/ positional encoding	16.394 ± 4.294	0.272 ± 0.041

Distribution analysis. In addition to summary statistics, we plot the distribution plot and box plot of RMSD and TM-scores across the dataset, figs. 3 and 4. These results reinforce the trends observed in table 2. The GCN model with positional encodings exhibits the most favourable distribution, with RMSD values concentrated toward lower errors and TM-scores shifted toward higher similarity. The UNet baseline, although simpler, produces a broader distribution with a heavier tail of poorly reconstructed examples. By contrast, the GCN without positional encodings consistently underperforms, with TM-scores clustered around low values and RMSD heavily shifted left, demonstrating that sequential information is critical for modelling backbone geometry.

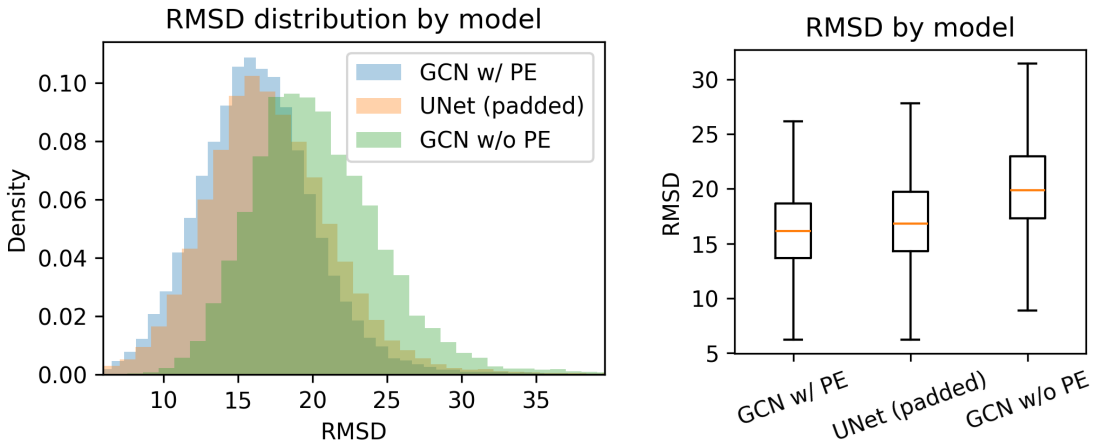

(a) Distribution of RMSD.

(b) Box plot of RMSD.

Figure 3: Distribution and box plot of RMSD values across test structures. Lower is better.

We further analyse model performance as a function of backbone length L, plotting RMSD and TM-score versus L in fig. 5. Both metrics exhibit a clear dependence on sequence length: reconstruction error (RMSD) increases with L, while TM-score tends to decrease for longer proteins. This trend reflects the inherent difficulty of maintaining structural fidelity over extended chains, where deviations accumulate and long-range dependencies become harder to capture.

Across all lengths, the GCN model with positional encodings achieves the best performance, with lower RMSD growth rates and consistently higher TM-scores. The UNet baseline performs comparably on shorter backbones but degrades more quickly as length increases, consistent with its reliance on fixed-length padded representations. The GCN without positional encodings consistently underperforms, with rapidly increasing RMSD

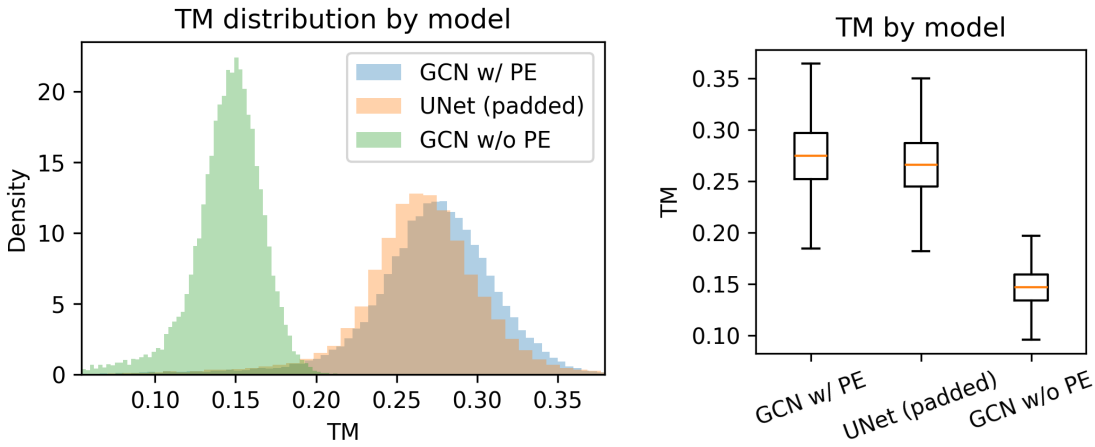

(a) Distribution of TM-score.

(b) Box plot of TM-score.

Figure 4: Distribution and box plot of TM-scores across test structures. Higher is better.

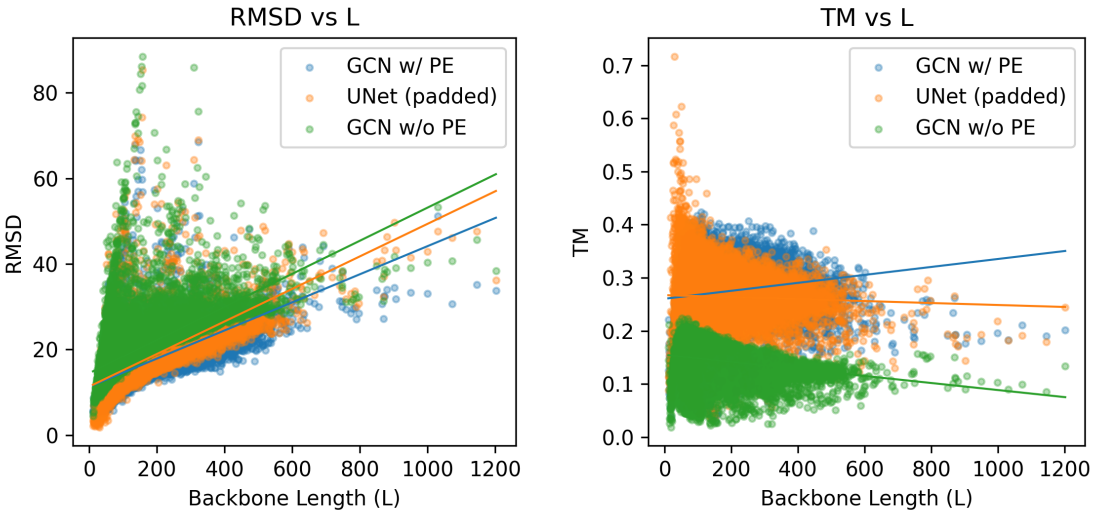

(a) RMSD vs. L.

(b) TM-score vs. L.

Figure 5: RMSD and TM-score versus backbone length L.

and TM-scores falling below 0.2 for most lengths, highlighting its inability to capture directional structure. These results emphasise that positional encodings are particularly critical for modelling long backbones, where sequential information provides essential constraints on geometry.

4.5 Qualitative Visualisation

We now present qualitative visualisations of generated backbones alongside a true native backbone, rendered in PyMOL (Schrödinger, LLC, 2015c,b,a). For each case, we display the C_α-trace of the generated structure together with the corresponding reference backbone (fig. 6). These visualisations provide an intuitive sense of how different architectures behave, illustrate both successful reconstructions, where the generated backbone closely follows the native fold (low RMSD, high TM-score), and failure cases, where the model produces geometrically plausible but non-native conformations.

The Transformer-based GCN with positional encodings produces generations that resemble the overall topology of the reference backbone, though with local deviations. The UNet baseline yields broadly plausible structures but can introduce artifacts, particularly in regions affected by padding. The GCN without positional encodings performs noticeably worse in this example, producing a collapsed global fold. While these individual cases are not sufficient for firm conclusions, they are broadly consistent with the quantitative trends: positional information improves global fold recovery, and its absence leads to systematic degradation. Together, these visualisations complement the statistical results by illustrating the kinds of conformations the models tend to generate.

4.6 Summary of Results

In summary, our experiments demonstrate that incorporating positional encodings into a Transformer-based graph neural network substantially improves backbone generation fidelity. Across quantitative metrics, the positional GCN achieved the lowest RMSD and highest TM-scores, outperforming both the UNet baseline and the GCN without positional information. Distributional analyses further showed that this model produces more consistent samples, while both quantitative results and qualitative visualisations highlighted that the absence of positional encodings often leads to collapsed or unrealistic folds.

At the same time, challenges remain. RMSD and TM-scores still indicate a gap between generated and native backbones, particularly for long chains where deviations accumulate. Individual qualitative examples provide intuition but do not fully capture the diversity of generated structures, suggesting the need for larger-scale structural assessments.

Overall, these results underscore the importance of combining geometric and sequential information when modelling proteins with diffusion processes. The following chapter discusses the broader implications of these findings, outlines limitations of the present work, and suggests directions for future research.

(a) True sample from CATH S40.

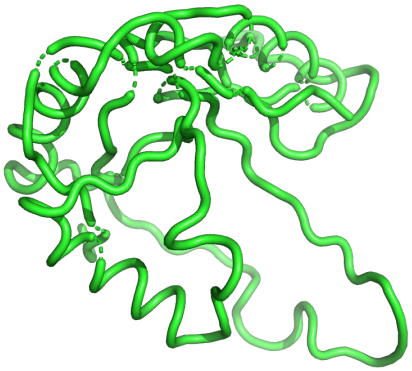

(b) Sample from Unet model.

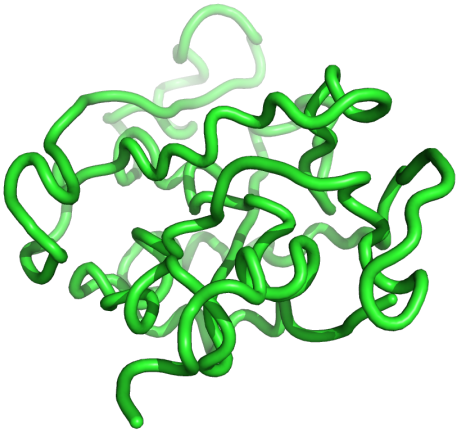

(c) Sample from GNN w/ positional encoding.

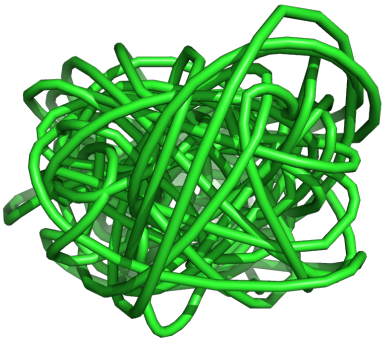

(d) Sample from GNN w/o positional encoding.

Figure 6: PyMOL visualisation of generated backbone samples from different models

5 Discussion and Conclusion

5.1 Discussion of Results

The experiments in Section 4 demonstrate that score-based diffusion models can generate protein backbones with meaningful structural similarity to native folds. Our main model, the TransformerConv GNN with positional embeddings, consistently outperformed the baselines in both RMSD and TM-score. This highlights the importance of incorporating sequential information into graph-based architectures, in addition to geometric edge features.

The ablation studies further show that GraphNorm provided more stable training than LayerNorm, particularly for variable-length proteins. Meanwhile, the UNet baseline performed poorly, underscoring the limitations of sequence-padded architectures that ignore protein geometry.

5.2 Limitations

While results are encouraging, several limitations must be acknowledged:

- **Evaluation metrics.** RMSD and TM-score measure similarity to a specific native fold of length L. However, a generated backbone with high RMSD or low TM may still correspond to a physically plausible alternative fold. Thus, our evaluation measures reconstruction fidelity rather than unconditional validity.
- **Backbone-only representation.** We model only C_α atoms, ignoring side chains and residue types. This limits biological interpretability and applicability to sequence-conditioned design.
- **Geometric constraints.** We did not enforce hard bond length or bond angle constraints during training or sampling. Although the model learns approximate geometry from data, explicit constraints would ensure chemical validity.
- **Model scale.** Our models are relatively small compared to state-of-the-art generative protein models. Larger networks with equivariant layers or global attention may further improve results.

5.3 Future Work

Several promising directions follow from this study:

- **Constraint integration.** Future models could enforce bond lengths, bond angles, and chirality constraints explicitly within the diffusion dynamics.
- **Sequence conditioning.** Extending the framework to sequence-to-structure generation would enable protein design tasks directly relevant to biology and drug discovery.
- **Advanced architectures.** Incorporating SE(3)-equivariant GNNs, Graph GPS layers, or global attention could capture long-range dependencies more effectively.

- **Evaluation metrics.** Beyond RMSD and TM-score, metrics that capture physical validity or functional plausibility would provide a more nuanced evaluation of generated backbones.

5.4 Conclusion

This dissertation has presented an adaptation of score-based diffusion models to the task of protein backbone generation. We derived the theoretical foundations of score-based diffusion, constructed graph-based representations of protein structures, and developed several neural architectures for score estimation. Through experiments on the CATH S40 dataset, we demonstrated that a residual TransformerConv GNN with positional embeddings achieves improved performance over both non-graph and graph baselines.

Overall, this work illustrates the potential of diffusion generative models for structural biology and provides a foundation for future research in protein design. By integrating probabilistic rigour with graph-based learning, score-based diffusion offers a principled and flexible framework for exploring the immense space of protein structures.

A Code Appendix

References

Anderson, B. D. O. (1982). Reverse-time diffusion equation models. *Stochastic Processes and their Applications*, 12(3):313–326.

Battaglia, P. W., Hamrick, J. B., Bapst, V., Sanchez-Gonzalez, A., Zambaldi, V., Malinowski, M., Tacchetti, A., Raposo, D., Santoro, A., Faulkner, R., Gulcehre, C., Song, F., Ballard, A., Gilmer, J., Dahl, G., Vaswani, A., Allen, K., Nash, C., Langston, V., Dyer, C., Heess, N., Wierstra, D., Kohli, P., Botvinick, M., Vinyals, O., Li, Y., and Pascanu, R. (2018). Relational inductive biases, deep learning, and graph networks.

Branden, C. I. and Tooze, J. (2012). *Introduction to Protein Structure*. Garland Science, New York, 2 edition.

Cai, T., Luo, S., Xu, K., He, D., Liu, T.-Y., and Wang, L. (2021). GraphNorm: A Principled Approach to Accelerating Graph Neural Network Training. In *Proceedings of the 38th International Conference on Machine Learning*, pages 1204–1215. PMLR.

Creighton, T. E. (1993). *Proteins: structures and molecular properties*. Macmillan.

Dhariwal, P. and Nichol, A. (2021). Diffusion Models Beat GANs on Image Synthesis. In *Advances in Neural Information Processing Systems*, volume 34, pages 8780–8794. Curran Associates, Inc.

Fey, M. and Lenssen, J. E. (2019). Fast graph representation learning with PyTorch Geometric. In *ICLR Workshop on Representation Learning on Graphs and Manifolds*.

Fey, M., Sunil, J., Nitta, A., Puri, R., Shah, M., Stojanovič, B., Bendias, R., Alexandria, B., Kocijan, V., Zhang, Z., He, X., Lenssen, J. E., and Leskovec, J. (2025). PyG 2.0: Scalable learning on real world graphs. In *Temporal Graph Learning Workshop @ KDD*.

Geiger, M. and Smidt, T. (2022). E3nn: Euclidean Neural Networks.

Geiger, M., Smidt, T., M, A., Miller, B. K., Boomsma, W., Dice, B., Lapchevskyi, K., Kotak, M., Tyszkiewicz, M., Uhrin, M., Batzner, S., Madisetti, D., Frellsen, J., Maheshkar, S., Jung, N., Fomitchev, B., Wen, M., jkh, Sanborn, S., Barnes, R., Kohler, C., Morehead, A., Tan, C. W., Rackers, J., LFu, Rød, M., Bailey, M., Brocidiacono, M., eszter137, and McConkey, R. (2025). Euclidean neural networks: E3nn. Zenodo.

Gilmer, J., Schoenholz, S. S., Riley, P. F., Vinyals, O., and Dahl, G. E. (2017). Neural Message Passing for Quantum Chemistry. In *Proceedings of the 34th International Conference on Machine Learning*, pages 1263–1272. PMLR.

Goodfellow, I., Pouget-Abadie, J., Mirza, M., Xu, B., Warde-Farley, D., Ozair, S., Courville, A., and Bengio, Y. (2020). Generative adversarial networks. *Commun. ACM*, 63(11):139–144.

He, K., Zhang, X., Ren, S., and Sun, J. (2016). Deep Residual Learning for Image Recognition. In *Proceedings of the IEEE Conference on Computer Vision and Pattern Recognition*, pages 770–778.

Ho, J., Jain, A., and Abbeel, P. (2020). Denoising Diffusion Probabilistic Models. In *Advances in Neural Information Processing Systems*, volume 33, pages 6840–6851. Curran Associates, Inc.

Hyvärinen, A. (2005). Estimation of Non-Normalized Statistical Models by Score Matching. *Journal of Machine Learning Research*, 6(24):695–709.

Jumper, J., Evans, R., Pritzel, A., Green, T., Figurnov, M., Ronneberger, O., Tunyasuvunakool, K., Bates, R., Žídek, A., Potapenko, A., Bridgland, A., Meyer, C., Kohl, S. A. A., Ballard, A. J., Cowie, A., Romera-Paredes, B., Nikolov, S., Jain, R., Adler, J., Back, T., Petersen, S., Reiman, D., Clancy, E., Zielinski, M., Steinegger, M., Pacholska, M., Berghammer, T., Bodenstein, S., Silver, D., Vinyals, O., Senior, A. W., Kavukcuoglu, K., Kohli, P., and Hassabis, D. (2021). Highly accurate protein structure prediction with AlphaFold. *Nature*, 596(7873):583–589.

Kingma, D. P. and Ba, J. (2017). Adam: A Method for Stochastic Optimization.

Kingma, D. P. and Welling, M. (2022). Auto-Encoding Variational Bayes.

Kipf, T. N. and Welling, M. (2017). Semi-Supervised Classification with Graph Convolutional Networks.

Lewis, T. E., Sillitoe, I., Dawson, N., Lam, S. D., Clarke, T., Lee, D., Orengo, C., and Lees, J. (2018). Gene3D: Extensive prediction of globular domains in proteins. *Nucleic Acids Research*, 46(D1):D435–D439.

Li, G., Muller, M., Thabet, A., and Ghanem, B. (2019). DeepGCNs: Can GCNs Go As Deep As CNNs? In *Proceedings of the IEEE/CVF International Conference on Computer Vision*, pages 9267–9276.

Li, Q., Han, Z., and Wu, X.-m. (2018). Deeper Insights Into Graph Convolutional Networks for Semi-Supervised Learning. *Proceedings of the AAAI Conference on Artificial Intelligence*, 32(1).

Nichol, A. and Dhariwal, P. (2021). Improved Denoising Diffusion Probabilistic Models.

Orengo, C. A., Michie, A. D., Jones, S., Jones, D. T., Swindells, M. B., and Thornton, J. M. (1997). CATH – a hierarchic classification of protein domain structures. *Structure*, 5(8):1093–1109.

Ronneberger, O., Fischer, P., and Brox, T. (2015). U-Net: Convolutional Networks for Biomedical Image Segmentation. In Navab, N., Hornegger, J., Wells, W. M., and Frangi, A. F., editors, *Medical Image Computing and Computer-Assisted Intervention – MICCAI 2015*, pages 234–241, Cham. Springer International Publishing.

Saharia, C., Chan, W., Saxena, S., Li, L., Whang, J., Denton, E. L., Ghasemipour, K., Gontijo Lopes, R., Karagol Ayan, B., Salimans, T., Ho, J., Fleet, D. J., and Norouzi, M. (2022). Photorealistic Text-to-Image Diffusion Models with Deep Language Understanding. *Advances in Neural Information Processing Systems*, 35:36479–36494.

Scarselli, F., Gori, M., Tsoi, A. C., Hagenbuchner, M., and Monfardini, G. (2009). The Graph Neural Network Model. *IEEE Transactions on Neural Networks*, 20(1):61–80.

Schrödinger, LLC (2015a). The AxPyMOL molecular graphics plugin for Microsoft PowerPoint, version 1.8. Website: https://pymol.org/axpymol.

Schrödinger, LLC (2015b). The JyMOL molecular graphics development component, version 1.8. Website: https://pymol.org/axpymol.

Schrödinger, LLC (2015c). The PyMOL molecular graphics system, version 1.8. Website: https://pymol.org/axpymol.

Senior, A. W., Evans, R., Jumper, J., Kirkpatrick, J., Sifre, L., Green, T., Qin, C., Žídek, A., Nelson, A. W. R., Bridgland, A., Penedones, H., Petersen, S., Simonyan, K., Crossan, S., Kohli, P., Jones, D. T., Silver, D., Kavukcuoglu, K., and Hassabis, D. (2020). Improved protein structure prediction using potentials from deep learning. *Nature*, 577(7792):706–710.

Shi, Y., Huang, Z., Feng, S., Zhong, H., Wang, W., and Sun, Y. (2021). Masked Label Prediction: Unified Message Passing Model for Semi-Supervised Classification.

Sillitoe, I., Bordin, N., Dawson, N., Waman, V. P., Ashford, P., Scholes, H. M., Pang, C. S. M., Woodridge, L., Rauer, C., Sen, N., Abbasian, M., Le Cornu, S., Lam, S. D., Berka, K., Varekova, I. H., Svobodova, R., Lees, J., and Orengo, C. A. (2021). CATH: Increased structural coverage of functional space. *Nucleic Acids Research*, 49(D1):D266–D273.

Song, Y., Durkan, C., Murray, I., and Ermon, S. (2021a). Maximum Likelihood Training of Score-Based Diffusion Models. In *Advances in Neural Information Processing Systems*, volume 34, pages 1415–1428. Curran Associates, Inc.

Song, Y., Sohl-Dickstein, J., Kingma, D. P., Kumar, A., Ermon, S., and Poole, B. (2021b). Score-Based Generative Modeling through Stochastic Differential Equations. In *International Conference on Learning Representations*.

Tancik, M., Srinivasan, P., Mildenhall, B., Fridovich-Keil, S., Raghavan, N., Singhal, U., Ramamoorthi, R., Barron, J., and Ng, R. (2020). Fourier Features Let Networks Learn High Frequency Functions in Low Dimensional Domains. In *Advances in Neural Information Processing Systems*, volume 33, pages 7537–7547. Curran Associates, Inc.

Vaswani, A., Shazeer, N., Parmar, N., Uszkoreit, J., Jones, L., Gomez, A. N., ukasz Kaiser, Ł., and Polosukhin, I. (2017). Attention is All you Need. In *Advances in Neural Information Processing Systems*, volume 30. Curran Associates, Inc.

Vincent, P. (2011). A Connection Between Score Matching and Denoising Autoencoders. *Neural Computation*, 23(7):1661–1674.

Waman, V. P., Bordin, N., Alcraft, R., Vickerstaff, R., Rauer, C., Chan, Q., Sillitoe, I., Yamamori, H., and Orengo, C. (2024). CATH 2024: CATH-AlphaFlow Doubles the Number of Structures in CATH and Reveals Nearly 200 New Folds. *Journal of Molecular Biology*, 436(17):168551.

Watson, J. L., Juergens, D., Bennett, N. R., Trippe, B. L., Yim, J., Eisenach, H. E., Ahern, W., Borst, A. J., Ragotte, R. J., Milles, L. F., Wicky, B. I. M., Hanikel, N., Pellock, S. J., Courbet, A., Sheffler, W., Wang, J., Venkatesh, P., Sappington, I., Torres, S. V., Lauko, A., De Bortoli, V., Mathieu, E., Ovchinnikov, S., Barzilay, R., Jaakkola, T. S., DiMaio,

F., Baek, M., and Baker, D. (2023). De novo design of protein structure and function with RFdiffusion. *Nature*, 620(7976):1089–1100.

Wu, K. E., Yang, K. K., van den Berg, R., Alamdari, S., Zou, J. Y., Lu, A. X., and Amini, A. P. (2024). Protein structure generation via folding diffusion. *Nature Communications*, 15(1):1059.

Xu, J. and Zhang, Y. (2010). How significant is a protein structure similarity with TM-score = 0.5? *Bioinformatics*, 26(7):889–895.

Yim, J., Stärk, H., Corso, G., Jing, B., Barzilay, R., and Jaakkola, T. S. (2024). Diffusion models in protein structure and docking. *WIREs Computational Molecular Science*, 14(2):e1711.

Zhang, Y. and Skolnick, J. (2004). Scoring function for automated assessment of protein structure template quality. *Proteins: Structure, Function, and Bioinformatics*, 57(4):702–710.

Zhang, Y. and Skolnick, J. (2005). TM-align: A protein structure alignment algorithm based on the TM-score. *Nucleic Acids Research*, 33(7):2302–2309.